
⁸⁹Zr-Nanocolloidal Albumin–Based PET/CT Lymphoscintigraphy for Sentinel Node Detection in Head and Neck Cancer: Preclinical Results

Derrek A. Heuveling¹, Gerard W.M. Visser², Marian Baclayon³, Wouter H. Roos³, Gijs J.L. Wuite³, Otto S. Hoekstra², C. René Leemans¹, Remco de Bree¹, and Guus A.M.S. van Dongen^{1,2}

¹Department of Otolaryngology/Head and Neck Surgery, VU University Medical Center, Amsterdam, The Netherlands; ²Department of Nuclear Medicine and PET Research, VU University Medical Center, Amsterdam, The Netherlands; and ³Department of Physics and Astronomy, VU University, Amsterdam, The Netherlands

Identifying sentinel nodes near the primary tumor remains a problem in, for example, head and neck cancer because of the limited resolution of current lymphoscintigraphic imaging when using ^{99m}Tc-nanocolloidal albumin. This study describes the development and evaluation of a nanocolloidal albumin–based tracer specifically dedicated for high-resolution PET detection. **Methods:** ⁸⁹Zr was coupled to nanocolloidal albumin via the bifunctional chelate *p*-isothiocyanatobenzylferrioxamine B. Quality control tests, including particle size measurements, and in vivo biodistribution and imaging experiments in a rabbit lymphogenic metastasis model were performed. **Results:** Coupling of ⁸⁹Zr to nanocolloidal albumin appeared to be efficient, resulting in a stable product with a radiochemical purity greater than 95%, without affecting the particle size. PET showed distinguished uptake of ⁸⁹Zr-nanocolloidal albumin in the sentinel nodes, with visualization of lymphatic vessels, and with a biodistribution comparable to ^{99m}Tc-nanocolloidal albumin. **Conclusion:** ⁸⁹Zr-nanocolloidal albumin is a promising tracer for sentinel node detection by PET.

Key Words: sentinel node; PET/CT; ⁸⁹Zr; Nanocoll; head and neck cancer

J Nucl Med 2011; 52:1580–1584

DOI: 10.2967/jnumed.111.089557

The sentinel node (SN) procedure is applied in a variety of tumor types, including head and neck squamous cell carcinoma (HNSCC) (1,2). Although, in general, results in HNSCC are good, adequate detection of the SN in floor-of-mouth tumors, compared with other sites, appeared problematic, as illustrated by significantly lower sensitivity and negative predictive value (1). This is probably due to the short distance between the primary tumor and the first draining lymph nodes (SNs) in combination with the limited resolution

of planar lymphoscintigraphy and SPECT. The injection site (around the primary tumor) produces a large focus of intense activity on planar lymphoscintigraphy, possibly hiding SNs near the primary tumor. As a result, second-echelon lymph nodes may erroneously be considered SNs; this is also true for SPECT: the added value of detecting foci hidden at planar scintigraphy may be offset by its lack of dynamic information with the typically fast kinetics of lymph drainage in HNSCC.

PET provides dynamic 3-dimensional information at a higher spatial resolution than achievable with a γ -camera. Theoretically, these characteristics may better differentiate between the first- and second-echelon nodes. To the best of our knowledge, no PET radiocolloids specifically dedicated to lymphatic mapping are clinically available yet. The aim of this study was to develop and evaluate in a rabbit lymphogenic metastasis model a ⁸⁹Zr (half-life, 78 h)-nanocolloidal albumin (Nanocoll; GE Healthcare)-based PET radiocolloid dedicated to SN detection. Results were compared with ^{99m}Tc-nanocolloidal albumin (^{99m}Tc half-life, 6 h).

MATERIALS AND METHODS

Preparation of ⁸⁹Zr- and ^{99m}Tc-Nanocolloidal Albumin

A 0.5-mg kit for the labeling of colloidal human serum albumin with ^{99m}Tc was premodified with *p*-isothiocyanatobenzylferrioxamine B (Df-Bz-NCS [Macrocyclics]) and labeled with ⁸⁹Zr (IBA Molecular) essentially according to the protocol in Table 1. ^{99m}Tc-nanocolloidal albumin was prepared according to the manufacturer's information (3).

Analysis

Labeling kinetics and radiochemical purity were determined by instant thin-layer chromatography using silica gel-impregnated glass fiber sheets (Gelman Sciences). For instant thin-layer chromatography analysis of ⁸⁹Zr-nanocolloidal albumin, citrate buffer (20 mmol/L, pH 5.0) with 10% acetonitrile was used as the mobile phase. For ^{99m}Tc-nanocolloidal albumin, the mobile phase was methanol:water (85:15 v/v). *R_f* values were 0–0.1 for ⁸⁹Zr/^{99m}Tc-nanocolloidal albumin and 0.7–1.0 for free ⁸⁹Zr/^{99m}Tc.

For comparison of the particle size of ⁸⁹Zr-nanocolloidal albumin and ^{99m}Tc-nanocolloidal albumin, both colloids were analyzed by atomic force microscopy (AFM), a single-particle technique that has successfully been used to characterize a wide variety of nano-

Received Feb. 21, 2011; revision accepted Jun. 22, 2011.

For correspondence or reprints contact: Guus A.M.S. van Dongen, Department of Otolaryngology/Head and Neck Surgery, VU University Medical Center, De Boelelaan 1117, P.O. Box 7057, 1007 MB Amsterdam, The Netherlands.

E-mail: gams.vandongen@vumc.nl

Published online Sep. 2, 2011.

COPYRIGHT © 2011 by the Society of Nuclear Medicine, Inc.

TABLE 1
Labeling Protocol of ^{89}Zr -Nanocolloidal Albumin

Step	Procedure
1	950 μL of polysorbate-citrate buffer*, pH 6.5, are added to 1 vial of nanocolloidal albumin (0.5 mg)
2	45 μL of 0.1 M Na_2CO_3 are added to reach a pH of 9
3	167 nmol of Df-Bz-NCS [†] are added in 20 μL of dimethyl sulfoxide (in 4 \times 5 μL steps)
4	Solution is incubated for 30 min at 37°C
5	Nonconjugated Df-Bz-NCS is removed by size-exclusion chromatography using 1 PD10 column (GE Healthcare) and polysorbate-citrate buffer, pH 6.5, as eluent [‡] <i>Modification is now complete, resulting in Df-Bz-NCS-nanocolloidal albumin</i>
6	200 μL of ^{89}Zr -oxalate [§] (20–25 MBq) are added to wobbling reaction vial
7	90 μL of 2 M Na_2CO_3 are added
8	After 3 min, the following solutions are added: 300 μL of 0.5 M <i>N</i> -(2-hydroxyethyl)piperazine- <i>N'</i> -(2-ethanesulfonic acid) buffer, pH 7.0; 710 μL of Df-Bz-NCS-nanocolloidal albumin (0.18 mg); and 700 μL of 0.5 M <i>N</i> -(2-hydroxyethyl)piperazine- <i>N'</i> -(2-ethanesulfonic acid) buffer, pH 7.0 Start of reaction, 0 min
9	At 60 min, reaction mixture is purified (1 PD10 column; eluent polysorbate-citrate buffer, pH 6.5) [†] <i>Labeling is now complete, resulting in ^{89}Zr-nanocolloidal albumin</i>

*This buffer consists of 7.35 mg of sodium citrate per milliliter, with 0.7 mg of polysorbate 80 per milliliter in deionized water, pH 6.5.

[†]167 nmol Df-Bz-NCS corresponds to 20-fold molar excess of Df-Bz-NCS to nanocolloidal albumin.

[‡]Elution pattern: flow-through and first 1.5 mL are discarded. Next 2 mL contain Df-Bz-NCS-nanocolloidal albumin (step 5) or ^{89}Zr -labeled nanocolloidal albumin (step 9).

[§] ^{89}Zr -oxalate in 1.0 M oxalic acid.

meter-sized proteinaceous assemblies (4–6). In addition, native nanocolloidal albumin in polysorbate-citrate buffer, pH 6.5, diluted to a concentration of 0.10 mg/mL, was included in this analysis to determine whether the modification of nanocolloidal albumin with Df-Bz-NCS and subsequent labeling with ^{89}Zr altered the particle size of the colloids. The atomic force microscope (Nanotec Electronica) was operated in jumping mode, and all experiments were performed in liquid. Rectangular cantilevers (RC800PSA; Olympus) with a nominal tip radius of 20 nm and spring constant of 0.05 N/m were used to image the colloid particles. Colloid samples were deposited on a freshly cleaved mica substrate and incubated for 10 min before they were analyzed by AFM. Height measurements on the immobilized particles were performed in an automated way (home-written program in LabView; National Instruments) to obtain the particle size distribution.

Rabbit VX2 Auricle Carcinoma Model

Female rabbits (HsdIf:NZW; Harlan Laboratories) bearing auricular VX2 carcinoma (Fig. 1) were used for in vivo evaluation of radiocolloids (7–9). VX2 tumor cells were kindly provided by Dr. Robert J.J. van Es (Department of Oral and Maxillofacial Surgery, University Medical Center Utrecht), and tumors were induced by injection of 0.15–0.25 mL containing $25\text{--}30 \times 10^6$ VX2 tumor cells in both ears. All animal experiments were performed in accordance with Dutch animal welfare regulations and Dutch national law (“Wet op de dierproeven,” Stb 1985, 336).

Imaging Experiments

Administration of radiocolloids occurred always via 3–4 peritumoral subcutaneous injections of 0.15–0.25 mL each. To evaluate the distribution of $^{99\text{m}}\text{Tc}$ -nanocolloidal albumin in the auricular VX2 carcinoma model, 4 tumor-bearing rabbits were unilaterally imaged using a γ -camera (e.cam dual-detector camera; Siemens Medical Solutions). Dynamic imaging was started

immediately after injection of $^{99\text{m}}\text{Tc}$ -nanocolloidal albumin (5–10 MBq) and consisted of 10 frames of 1 min. Static images were acquired at 10 min after injection.

PET (HRRT PET scanner; Siemens/CTI) (10) or PET/CT (Gemini TF64; Philips) (11) was performed on 6 rabbits with

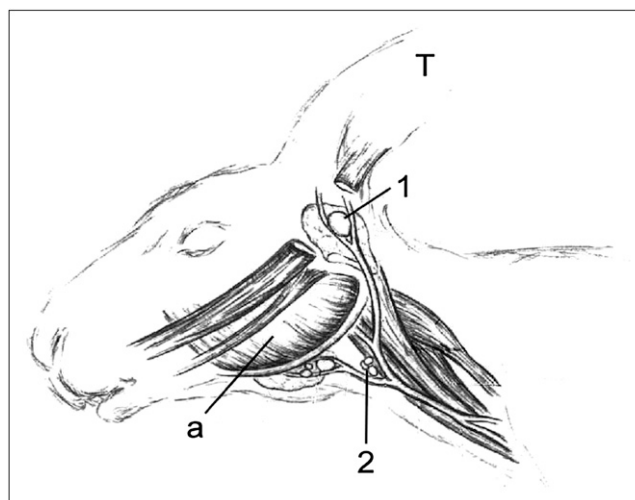


FIGURE 1. Rabbit VX2 auricular carcinoma model. This animal model is attractive for evaluating SN detection procedures in HNSCC, because after inoculation of tumor cells into ear, arising tumors (T) tend to metastasize lymphatically. First lymph node that will be metastatically involved within about 21 d, SN, is parotid lymph node (1). Caudal mandibular lymph nodes (2) are second-echelon lymph nodes in this model. Consistent lymphogenic metastatic spread of tumor and accessibility of lymph nodes for surgery makes this a suitable model for evaluation of SN detection. a = angle of mandible.

tumors in both ears ($n = 12$). Two animals received only ^{89}Zr -nanocolloidal albumin (5 MBq), and the other 4 rabbits were injected with a mixture of ^{89}Zr - and $^{99\text{m}}\text{Tc}$ -nanocolloidal albumin (5–10 MBq each). Coinjection with $^{99\text{m}}\text{Tc}$ -nanocolloidal albumin was performed to allow for comparative biodistribution studies. No substantial interference of $^{99\text{m}}\text{Tc}$ during PET was anticipated. Dynamic imaging was started immediately after injection and consisted of a 1-h scan sorted into 26 frames (12×5 s, 4×15 s, 3×60 s, and 3×900 s).

Biodistribution Study

To compare the biodistribution of ^{89}Zr -nanocolloidal albumin with the reference $^{99\text{m}}\text{Tc}$ -nanocolloidal albumin, both radiocolloids were coinjected around 12 tumors in 6 rabbits. Two animals were euthanized 30 min after coinjection of the radiocolloids, without PET, and the other 4 animals were euthanized after the imaging experiments were finished—that is, at 1 and 3 h after injection. After preparation of a skin flap, enlarged parotid and caudal mandibular lymph nodes were identified and harvested bilaterally. Besides the lymph nodes, the following nonlymphatic tissues were removed: skin and muscle from the hind limb, heart, lung, liver, spleen, and sternum. Blood was also collected. After weighing, radioactivity in each sample was assessed in a γ -counter (Wallac), using the corresponding window settings for $^{99\text{m}}\text{Tc}$ and ^{89}Zr (for the 140- and 909-keV γ -energy, respectively). In this dual-isotope measurement, corrections for crossover from ^{89}Zr into the $^{99\text{m}}\text{Tc}$ window were performed using a standard of each radionuclide. Radioactivity uptake was calculated as the percentage injected dose per gram of tissue (%ID/g), corrected for radioactive decay.

Statistics

The square of Pearson correlation coefficient r (R^2 , determined using Excel [Microsoft]) was used to study the correlation between tissue uptake of ^{89}Zr -nanocolloidal albumin and $^{99\text{m}}\text{Tc}$ -nanocolloidal albumin.

RESULTS

Radiolabeling

Labeling of premodified nanocolloidal albumin (180 μg) with ^{89}Zr proved reproducible, with an overall labeling yield of 70%–75%. After PD10 purification, radiochemical purity always exceeded 95% and remained stable on storage for at least 24 h. Labeling of native nanocolloidal albumin, that is, without premodification with the Df-Bz-NCS chelate, showed less than 1% labeling. Labeling of nanocolloidal albumin with $^{99\text{m}}\text{Tc}$ resulted in a labeling yield and radiochemical purity greater than 95%. The plots of the particle size distribution are shown in Figure 2. The average size of the ^{89}Zr -nanocolloidal albumin particles was 12.7 ± 0.6 nm; for $^{99\text{m}}\text{Tc}$ -nanocolloidal albumin, this was 14.9 ± 0.5 nm, and for native nanocolloidal albumin, 13.8 ± 0.8 nm.

Imaging Studies

In all tumors injected with either $^{99\text{m}}\text{Tc}$ -nanocolloidal albumin or ^{89}Zr -nanocolloidal albumin, drainage occurred rather fast: within 5 min after injection, 2 foci of intense activity were already visible on planar lymphoscintigraphy (Fig. 3A) and on PET images (Fig. 3B), their localizations corresponding to the parotid and caudal mandibular lymph

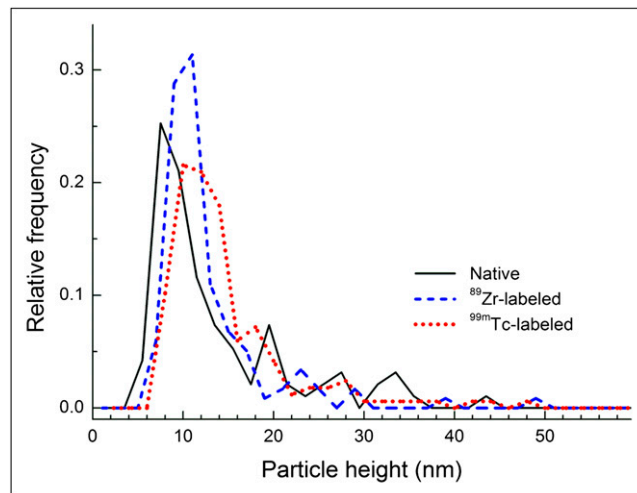


FIGURE 2. Size distribution of ^{89}Zr -labeled, $^{99\text{m}}\text{Tc}$ -labeled, and unlabeled (native) nanocolloidal albumin particles as assessed by AFM imaging. Number of analyzed particles for ^{89}Zr -nanocolloidal albumin was 112; for $^{99\text{m}}\text{Tc}$ -nanocolloidal albumin, 167; and for native nanocolloidal albumin, 95. AFM measures height of particle, which is representative measure for particle size.

nodes. As could be seen on dynamic images, the parotid lymph node indeed appeared to be the first draining lymph node and was best demonstrated by PET because with this technique, 3-dimensional images providing high-resolution visualization of connecting lymphatic vessels are acquired (Fig. 4). No other lymph nodes were visualized on any of the images. On all images, a slight uptake of radioactivity in the liver and spleen, explained by the known catabolic route of nanocolloidal albumin, was observed (3).

Biodistribution Studies

Results of tissue uptake of $^{99\text{m}}\text{Tc}$ - and ^{89}Zr -nanocolloidal albumin are presented in Table 2. Uptake in the lymph

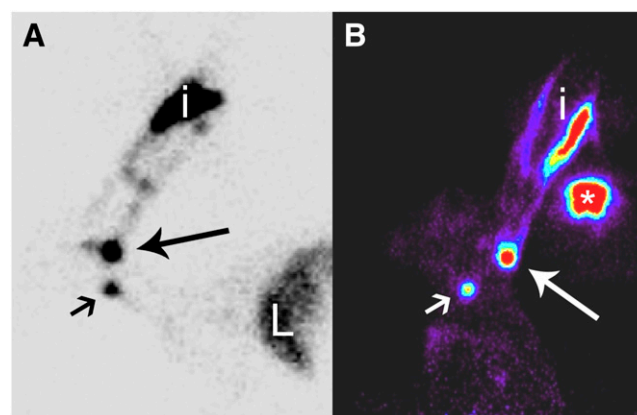


FIGURE 3. (A) Static planar lymphoscintigraphy image (10 min after injection of $^{99\text{m}}\text{Tc}$ -nanocolloidal albumin). (B) PET image (15 min after injection of ^{89}Zr -nanocolloidal albumin). In this slide, contralateral injection site (*) is also visible. On both images, parotid lymph node (large arrow) and caudal mandibular lymph node (small arrow) are clearly visible. i = injection site; L = liver.

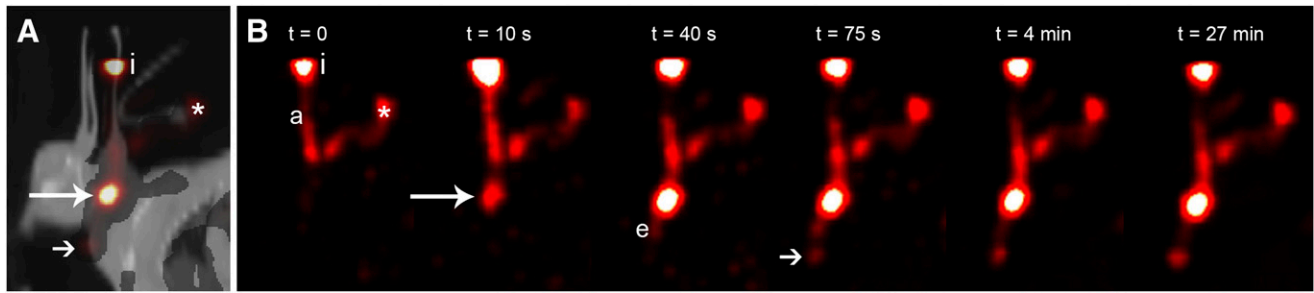


FIGURE 4. (A) PET/CT image 30 min after injection (i) of ^{89}Zr -nanocolloidal albumin around left ear tumor. (B) Dynamic PET images after injection of ^{89}Zr -nanocolloidal albumin around left ear tumor. Afferent (a) and efferent (e) lymphatic vessels are clearly visible in time, allowing identification of true SN. Contralateral injection site (*) with draining lymphatic vessel, which was injected earlier, is also visible in this slide. Uptake of ^{89}Zr -nanocolloidal albumin in sentinel lymph node (large arrow) and second-echelon lymph node (small arrow) is clearly visible on both images.

nodes was similar, ranging from 0.2 to 58.6 %ID/g and 0.2 to 60.2 %ID/g for ^{89}Zr -nanocolloidal albumin and $^{99\text{m}}\text{Tc}$ -nanocolloidal albumin, respectively, with a Pearson correlation coefficient r of 0.975 ($R^2 = 0.95$). Low uptake of both radiocolloids was observed in nonlymphatic tissues, with some isotope-specific differences.

DISCUSSION

In the present study, we describe a method for efficient and inert labeling of nanocolloidal albumin with ^{89}Zr using the bifunctional desferal chelate Df-Bz-NCS, which was previously introduced for the coupling of ^{89}Zr to intact monoclonal antibodies (12,13). Stable ^{89}Zr -nanocolloidal albumin radiocolloid was produced using this method. The developed labeling conditions did not affect the particle size, an important parameter that mainly determines kinetics and lymphatic uptake of the radiocolloid (14). In addition, uptake of ^{89}Zr -nanocolloidal albumin in the draining lymph nodes as observed in PET and biodistribution experiments was fully consistent with $^{99\text{m}}\text{Tc}$ -nanocolloidal albumin uptake.

For the premodification of nanocolloidal albumin, an important factor appeared to be the pH, which should be

greater than 6.0 to avoid precipitation of the colloid. For this reason, the tetrafluorophenol-*N*-succinyl-desferal (TFP-*N*-sucDf) chelate, which has been used for coupling of ^{89}Zr to proteins before, could not be used (15). The TFP-*N*-sucDf route requires a step at pH 4.0 to remove stable iron (Fe[III]) from the temporarily filled Df chelate and therefore appeared unsuitable for nanocolloidal albumin. The Df-Bz-NCS chelate, however, allows a simple labeling procedure consisting of premodification of nanocolloidal albumin at a pH of 9.0, labeling of Df-Bz-NCS-nanocolloidal albumin with ^{89}Zr at a pH of 7.0, and storage of ^{89}Zr -nanocolloidal albumin in polysorbate-citrate buffer at a pH of 6.5. No difficulties were observed with respect to precipitation of nanocolloidal albumin following this route, and ^{89}Zr -nanocolloidal albumin with a radiochemical purity greater than 95% can be produced.

With the introduction of SPECT/CT, functional and anatomic information has become available at the same time. In general, more SNs are identified by SPECT/CT than by planar lymphoscintigraphy (16–20). However, it may remain difficult or impossible to establish which are true SNs rather than second-echelon ones. The ultimate proof of whether a focus is an SN is visualization of an

TABLE 2
Tissue Uptake of $^{99\text{m}}\text{Tc}$ - and ^{89}Zr -Nanocolloidal Albumin

Tissue	No. of samples	%ID/g $^{99\text{m}}\text{Tc}$ -nanocolloidal albumin (mean \pm SEM)	%ID/g ^{89}Zr -nanocolloidal albumin (mean \pm SEM)	R^2 *
Lymph node				
Parotid lymph node	12	10.5 \pm 9.4	10.4 \pm 10.1	0.99
Caudal mandibular lymph node	12	23.5 \pm 18.1	20.0 \pm 18.1	0.95
Nonlymphatic tissue				
Liver	6	0.219 \pm 0.158	0.233 \pm 0.100	0.93
Spleen	6	0.397 \pm 0.056	0.412 \pm 0.054	0.86
Lung	6	0.017 \pm 0.009	0.017 \pm 0.008	0.63
Sternum	6	0.019 \pm 0.020	0.019 \pm 0.015	0.93
Skin	6	0.007 \pm 0.007	0.005 \pm 0.005	0.82
Muscle	6	0.004 \pm 0.005	0.003 \pm 0.005	0.96
Blood	6	0.012 \pm 0.008	0.009 \pm 0.003	0.55

* R^2 is correlation between uptake of $^{99\text{m}}\text{Tc}$ -nanocolloidal albumin and ^{89}Zr -nanocolloidal albumin.

afferent lymphatic vessel. Hence if more than 1 lymph node is labeled, dynamic imaging is required for interpretation, as is feasible with PET (Fig. 4). With respect to the identification of SNs adjacent to the primary tumor, that is, floor-of-mouth tumors, the additional value of SPECT/CT seemed to be limited (20). It remains to be shown whether the spatial resolution of PET will indeed improve the feasibility of SN detection in floor-of-mouth tumors.

Because nanocolloidal albumin is widely accepted for human use, and the developed ^{89}Zr -labeling procedure is compliant with good manufacturing practices, starting clinical studies with ^{89}Zr -nanocolloidal albumin should be easy. The use of a radionuclide with a long half-life could be justified by the low amount of radioactivity (i.e., ~ 5 MBq) that is needed to obtain satisfactory imaging results. This 5 MBq of ^{89}Zr corresponds to an effective dose equivalent of 0.15 mSv, whereas the effective dose is 0.44 mSv for the 110 MBq of $^{99\text{m}}\text{Tc}$ -nanocolloidal albumin that is normally used for SN detection.

CONCLUSION

This study describes the production and preclinical evaluation of ^{89}Zr -nanocolloidal albumin, a PET tracer specifically dedicated to lymphoscintigraphy by PET/CT. No differences were observed between ^{89}Zr - and $^{99\text{m}}\text{Tc}$ -nanocolloidal albumin regarding radiochemical purity, particle size, SN detection by imaging, and uptake in the regional lymph nodes, indicating the inertness of coupling of ^{89}Zr to nanocolloidal albumin. These results justify evaluation of ^{89}Zr -nanocolloidal albumin in a clinical setting.

DISCLOSURE STATEMENT

The costs of publication of this article were defrayed in part by the payment of page charges. Therefore, and solely to indicate this fact, this article is hereby marked "advertisement" in accordance with 18 USC section 1734.

ACKNOWLEDGMENTS

We thank Drs. Tobias Murthum and Prof. Jochen Werner (Otolaryngology/Head and Neck Surgery, University of Marburg, Germany) for their assistance during set-up of the animal model. Furthermore, we thank Klaas-Walter Meijer, Jerry Middelberg, and Paul Sinnige of the animal facility at the VU University Medical Center and Marijke Stigter-van Walsum (Otolaryngology/Head and Neck Surgery, VU University Medical Center) for their excellent support in the performance of the animal experiments and Inge De Greeuw, Mariska Verlaan, and Dr. Carla Molthoff (Nuclear

Medicine and PET Research, VU University Medical Center) for PET analysis. No other potential conflict of interest relevant to this article was reported.

REFERENCES

1. Alkureishi LWT, Ross GL, Shoaib T, et al. Sentinel node biopsy in head and neck squamous cell cancer: 5-year follow-up of a European multicenter trial. *Ann Surg Oncol*. 2010;17:2459–2464.
2. Paleri V, Rees G, Arullendran P, Shoaib T, Krishnan S. Sentinel node biopsy in squamous cell cancer of the oral cavity and oral pharynx: a diagnostic meta-analysis. *Head Neck*. 2005;27:739–747.
3. GE Healthcare. *Summary of Product Characteristics Nanocoll*. Eindhoven, The Netherlands: GE Healthcare; August 2010.
4. Binnig G, Quate CF, Gerber C. Atomic force microscope. *Phys Rev Lett*. 1986;56:930–933.
5. Baclayon M, Wuite GJL, Roos WH. Imaging and manipulation of single viruses by atomic force microscopy. *Soft Matter*. 2010;6:5273–5285.
6. Hansma HG, Kim KJ, Laney DE, et al. Properties of biomolecules measured from atomic force microscope images: a review. *J Struct Biol*. 1997;119:99–108.
7. Van Es RJJ, Dullens HFJ, Van der Bilt A, Koole R, Slootweg PJ. Evaluation of the VX2 rabbit auricle carcinoma as a model for head and neck cancer in humans. *J Craniomaxillofac Surg*. 2000;28:300–307.
8. Dünne AA, Mandic R, Ramaswamy A, et al. Lymphogenic metastatic spread of auricular VX2 carcinoma in New Zealand White rabbits. *Anticancer Res*. 2002;22:3273–3280.
9. Dünne AA, Plehn S, Schulz S, et al. Lymph node topography of the head and neck in New Zealand White rabbits. *Lab Anim*. 2003;37:37–43.
10. De Jong HWAM, Van Velden FHP, Kloet RW, Buijs FL, Boellaard R, Lammertsma AA. Performance evaluation of the ECAT HRRT: an LSO-LYSO double layer high resolution, high sensitivity scanner. *Phys Med Biol*. 2007;52:1505–1526.
11. Surti S, Kuhn A, Werner ME, Perkins AE, Kolthammer J, Karp JS. Performance of Philips Gemini TF PET/CT scanner with special consideration for its time-of-flight imaging capabilities. *J Nucl Med*. 2007;48:471–480.
12. Vosjan MJWD, Perk LR, Visser GWM, et al. Conjugation and radiolabeling of monoclonal antibodies with zirconium-89 for PET imaging using the bifunctional chelate p-isothiocyanatobenzyl-desferrioxamine. *Nat Protoc*. 2010;5:739–743.
13. Perk LR, Vosjan MJWD, Visser GWM, et al. p-Isothiocyanatobenzyl-desferrioxamine: a new bifunctional chelate for facile radiolabeling of monoclonal antibodies with zirconium-89 for immuno-PET imaging. *Eur J Nucl Med Mol Imaging*. 2010;37:250–259.
14. Bergqvist L, Strand SE, Persson BRR. Particle sizing and biokinetics of interstitial lymphoscintigraphic agents. *Semin Nucl Med*. 1983;13:9–19.
15. Verel I, Visser GWM, Boellaard R, Stigter-van Walsum M, Snow GB, Van Dongen GAMS. ^{89}Zr immuno-PET: comprehensive procedures for the production of ^{89}Zr -labeled monoclonal antibodies. *J Nucl Med*. 2003;44:1271–1281.
16. Even-Sapir E, Lerman H, Lievshitz G, et al. Lymphoscintigraphy for sentinel node mapping using a hybrid SPECT/CT system. *J Nucl Med*. 2003;44:1413–1420.
17. Wagner A, Schicho K, Glaser C, et al. SPECT-CT for topographic mapping of sentinel lymph nodes prior to gamma probe-guided biopsy in head and neck squamous cell carcinoma. *J Craniomaxillofac Surg*. 2004;32:343–349.
18. Bilde A, Von Buchwald C, Mortensen J, et al. The role of SPECT-CT in the lymphoscintigraphic identification of sentinel nodes in patients with oral cancer. *Acta Otolaryngol*. 2006;126:1096–1103.
19. Keski-Säntti H, Mätzke S, Kauppinen T, Törnwall J, Atula T. Sentinel lymph node mapping using SPECT-CT fusion imaging in patients with oral cavity squamous cell carcinoma. *Eur Arch Otorhinolaryngol*. 2006;236:1008–1012.
20. Haerle SK, Hany TF, Strobel K, Sidler D, Stoeckli SJ. Is there an additional value of SPECT/CT over planar lymphoscintigraphy for sentinel node mapping in oral/oropharyngeal squamous cell carcinoma? *Ann Surg Oncol*. 2009;16:3118–3124.